

Neutron star pulse profile observations as extreme gravity probes

Hector O. Silva* and Nicolás Yunes†

eXtreme Gravity Institute, Department of Physics, Montana State University, Bozeman, Montana 59717 USA
(Dated: August 19, 2019)

The x-ray emission of hot spots on the surface of neutron stars is the prime target of the *Neutron star Interior Composition Explorer* (NICER). These x-ray pulse profiles not only encode information of the bulk properties of these stars, which teaches us about matter at supranuclear densities, but also about the spacetime curvature around them which teaches us about relativistic gravity. We explore the possibility of performing strong-gravity tests with NICER observations using a recently developed pulse profile model beyond general relativity. Our results suggest that NICER can in principle place constraints on deviations from general relativity due to an additional scalar degree of freedom which are independent and competitive relative to constraints with binary pulsar observations.

I. INTRODUCTION

Extreme and mysterious, neutron stars are an unavoidable consequence of general relativity at high enough densities. With typical masses between 1 and 2 M_{\odot} , but radii of only ~ 11 km, their energy densities can exceed nuclear saturation in their inner core. When this occurs, matter can transmute into exotic forms that are impossible to replicate in laboratories on Earth, and understanding the physics of such extreme matter remains an open problem in nuclear astrophysics.

Neutron stars are not just a laboratory for nuclear physics. Their high densities also imply strong gravitational fields that exceed those that can be probed in the Solar System by seven orders of magnitude. Understanding the physics of such strong gravity objects requires the use of a relativistic theory of gravity, like general relativity [1]. Neutron star observations can therefore provide invaluable clues about both nuclear astrophysics and relativistic gravity, as was achieved with the recent observation of gravitational waves from the merger of two neutron stars [2–4].

We here report on the first results of a new program to systematically study how strong-field gravity can be probed with a particular set of neutron star observations: pulse profiles emitted by radiating hot spots on the star’s surface [5]. Neutron stars can have hot spots on their surface, i.e. regions where the surface temperature is much higher than the average, due to the impact of accreted material that is pulled in from a nearby, less dense star or by localized heating due to magnetospheric currents (see e.g. [6–10]). These hot spots rotate rapidly with the star, emitting x-rays that trace the spacetime geometry as they leave the star, producing a pulse profile upon detection. NASA’s *Neutron star Interior Composition Explorer* (NICER) is currently detecting these pulse profiles with unprecedented (timing) resolution through rotation-resolved spectroscopy of thermal and non-thermal emission [11–13]. Can NICER constrain (or reveal) deviations from general relativity in the strong-field regime of neutron stars?

The constraining power of such observations depend sensitively on our ability to accurately model the pulse profile within and outside general relativity. In [14] we presented a complete toolkit to model x-ray pulse profiles in an entire class of well-motivated modifications to general relativity: scalar-tensor gravity [15–17]. In this class, gravity is still described by the curvature of spacetime, characterized by the spacetime metric as in general relativity, but the metric is influenced by a scalar field that can be excited in sufficiently dense environments, as in neutron stars. Since the scalar field is usually negligible in the Solar System, scalar-tensor theories have survived a plethora of experimental tests [18], while remaining prime candidates for tests with neutron stars [19–21].

The toolkit is fast, computationally efficient, covers a generic family of scalar-tensor theories of gravity and it is ready to use for probing strong gravity with NICER observations. The resulting pulse profiles include Doppler shifts, relativistic aberration and time-delay effects, thus extending the work of [22] to scalar-tensor theories and the work of [23] to the required level of astrophysical realism. These effects are crucial for constructing sufficiently accurate pulse-profile models, thus enabling, for the first time, a serious data analysis investigation of the strength with which NICER observations can probe strong gravity. As a first step toward such an investigation, we present an approximate, restricted Bayesian calculation and find that a NICER observation consistent with general relativity could allow for constraints on scalar tensor theories that can be comparable to the most stringent constraints from binary pulsar observations to date [24–27].

II. LIGHT CURVE MODELING IN SCALAR-TENSOR GRAVITY

The x-ray photons emitted by hot spots at the surface of a neutron star trace its exterior spacetime geometry. If the star is isolated, or if its companion is far away and we focus on the neutron star’s vicinity, the exterior spacetime can be well-approximated by the Schwarzschild spacetime, provided the star rotates much slower than the Kepler limit; this is indeed the case for some targets of NICER, which have spin frequencies below 300 Hz. In scalar-tensor gravity, the gravi-

* hector.okadadasilva@montana.edu

† nicolas.yunes@montana.edu

tational interaction is mediated by a scalar field φ in addition to the usual metric tensor $g_{\mu\nu}$ of general relativity. Here we consider a wide class of theories in which a massless scalar field is minimally coupled to gravity, yet matter fields are coupled to the product of the function $A(\varphi)$ and the metric tensor $g_{\mu\nu}$. The function A determines the scalar-tensor model under consideration. The presence of the scalar field modifies the exterior spacetime of a static, spherically symmetric star which is no longer the usual Schwarzschild spacetime of general relativity, but instead is the Just spacetime [15, 28]. This spacetime depends not only on the baryonic mass of the star m , but also on the “charge” or field strength q of the scalar field φ . The modifications relative to the Schwarzschild spacetime are controlled by the scalar-charge-to-mass ratio $Q \equiv qc^2/(Gm)$ [15, 28], which is zero in general relativity. See [14] for a detailed discussion.

As a concrete example of scalar-tensor gravity we consider the two-parameter theory of [29, 30] in which $\ln A(\varphi) \equiv \alpha_0\varphi + \beta_0\varphi^2/2$. The parameter α_0 is related to the Brans-Dicke parameter ω_{BD} via $\alpha_0^2 = 1/(2\omega_{\text{BD}} + 3)$, and it is stringently constrained to $\alpha_0 \lesssim 3.4 \times 10^{-3}$ by Shapiro time-delay measurements of the Cassini spacecraft [31]. On the other hand, β_0 is unconstrained by Solar System experiments. When $\beta_0 \gtrsim -4.35$, neutron stars have a small $Q \propto \alpha_0$ [32] and they are similar to those of general relativity. When $\beta_0 \lesssim -4.35$ [33, 34], regardless of the equation of state (EoS) [35], the theory admits a new branch of solutions, where stars with $Q \approx O(1)$ are energetically favored over their general relativity counterparts, due to a non-perturbative effect called spontaneous scalarization¹ [29, 30]. Numerically integrating the stellar structure equations in this theory, we obtain m , q and $A(\varphi)$, which completely determine the spacetime. Figure 1 shows that the scalar field can significantly modify the stellar structure and thus the spacetime around it.

With the spacetime geometry at hand, we can construct a pulse profile model. In general relativity, the models used for NICER data analysis are semi-analytic, as full null geodesic ray tracing for the construction of millions of profiles in a Markov-Chain Monte-Carlo exploration of the likelihood is computationally prohibitive. A simple yet accurate model commonly used in general relativity is Schwarzschild+Doppler [22, 43, 44], whose generalization to scalar-tensor theory leads to the “Just+Doppler” model [14], which includes Schwarzschild+Doppler in the $Q = 0$ limit. As in the Schwarzschild+Doppler case, the Just+Doppler model is constructed under some simplifications: the star is assumed spherical (i.e. deformations due to rotation are ignored) and the effects of frame-dragging in the photon’s geodesic are neglected. As in general relativity, these effects

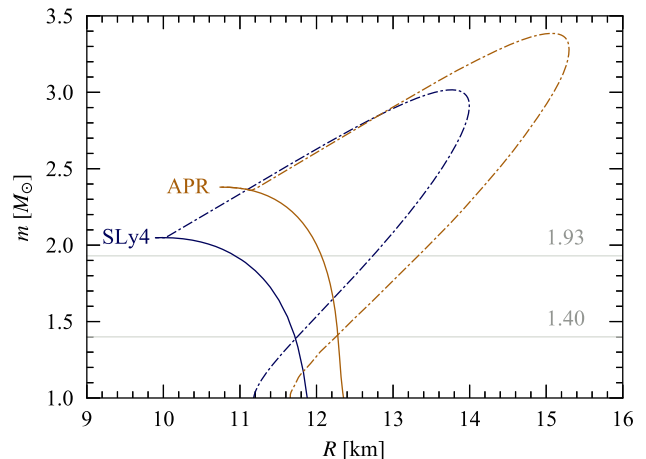


FIG. 1. Masses and radii of neutron stars in scalar-tensor gravity. The solid curves represent families of stars with varying central density in general relativity using the SLy4 [41] and APR [42] equations of state. Neutron stars in scalar-tensor gravity with fixed $\alpha_0 = 10^{-5}$ and $\beta_0 = -7$ are shown with dot-dashed curves, which bound the scalarized solutions (at fixed α_0) with increasing $|\beta_0|$. The value $\beta_0 = -7$ is ruled-out by binary pulsar observations, yet we include it here as an illustration of how large the deviations from general relativity can be in scalar-tensor theories which admit spontaneous scalarization. When β_0 is close to the scalarization threshold (i.e. ≈ -4.35) the differences between the general relativity and scalar-tensor gravity predictions for the mass-radius curves are negligible independently of the equation of state. The horizontal lines indicate that, given an EoS, neutron stars with larger mass (or equivalently larger central densities) have greater variation in their radius as β_0 becomes more negative.

in scalar-tensor theory are likely to have a negligible influence on the resulting pulse profile, as long as the star rotates slowly ($\lesssim 300$ Hz). This is because for slowly-rotating stars we do not expect much of a deformation away from sphericity due to rotation. Moreover, the frame-dragging of inertial frames in scalar-tensor gravity is very similar to that of general relativity, justifying extrapolating the conclusions from one theory to the other [45].

For our analysis, we further assume that the hot spot is small (relative to the size of the star) and isotropically radiating. In particular, we assume that the spot has a small angular radius $\Delta\theta$ and that it irradiates with a blackbody spectrum of constant $k_B T$ measured in the frame comoving with the hot spot (k_B being Boltzmann’s constant), while the rest of the star is dark. As often done in the literature, we consider a single hot spot (see e.g. [46, 47]) and (for simplicity) neglect any other radiation coming from the background. Finally, we assume that the observer collects photons in the soft x-ray band in a single energy channel of 1 keV. Although these simplifications are too rough to be implemented directly in an actual analysis of NICER data [48–52], they are sufficient for a first data analysis study, as shown through numerical simulations [46] and analytical estimates [53].

In scalar-tensor gravity, the model for the pulse profile depends not only on the parameters $\theta =$

¹ When the cosmological evolution of the scalar field is taken into account, $\beta < 0$ violates current Solar System constraints unless one fine-tunes the initial conditions for the cosmological evolution. When $\beta_0 > 0$, these constraints are satisfied [36] at the cost of disallowing scalarization, unless $\beta_0 \gtrsim 100$ [37]. We here study this theory with $\beta < 0$ as a toy-model for non-perturbative strong-gravity effects, generically predicted in gravitational theories with extra degrees of freedom (see e.g. [38–40]), and because it allows for comparison with binary pulsar constraints [24, 26].

$\{m, \theta_s, \iota_o, \Delta\theta, D, k_B T, f, \text{EoS}\}$ that describe the source, its geometry and the observer in general relativity, but also on the theory parameters α_0 (we use $\log_{10} |\alpha_0|$ in practice) and β_0 . In this parameter space, m is the mass of the star, which given a specified EoS determines its radius R , D is the distance to the source, f is the star's rotation frequency, θ_s is the colatitude of the center of the hotpot and ι_o is the inclination of the line of sight, both angles measured relative to the star's rotation axis. Since we must first calculate neutron star models in scalar-tensor gravity, instead of using m we use the central energy density $\varepsilon_{15} \equiv \varepsilon_c \times 10^{-15} \text{ g/cm}^{-3}$ as our model parameter. In summary, our full set of model parameters are $\theta = \{\varepsilon_{15}, \theta_s, \iota_o, \Delta\theta, D, k_B T, f, \text{EoS}, \log_{10} |\alpha_0|, \beta_0\}$.

III. PROJECTED CONSTRAINTS FROM OBSERVATIONS

Given the model described above, let us now roughly estimate the accuracy to which scalar-tensor theories could be constrained given a NICER observation that *is consistent with general relativity*. That is, we generate a synthetic signal (or injection) \mathbf{d} using the Schwarzschild+Doppler model in general relativity, and we then attempt to extract it and estimate its parameters with the Just+Doppler model.

A detailed analysis of the full likelihood is important, but beyond the scope of this work if one is concerned only with forecasting preliminary constraints. If the *forecasted constraints were to reveal that NICER cannot place interesting bounds on scalar-tensor gravity, then a more detailed analysis would not be necessary*. However, in the opposite case, one would conclude that NICER may be used as a laboratory to test general relativity, and a more detailed data analysis study would be justified. As we will show next, the latter is the case here.

The parameter space of the model is ten-dimensional and thus, to arrive at a rough estimate on projected constraints, we make a few simplifications that reduce this dimensionality. We fix $\{\theta_s, \iota_o, \Delta\theta, D, k_B T, f, \text{EoS}\}$ at their injected values (indicated by asterisks). For the first five, we set $\{\theta_s^*, \iota_o^*, \Delta\theta^*, D^*, k_B T^*\} = \{90^\circ, 90^\circ, 0.01^\circ, 600 \text{ pc}, 0.35 \text{ keV}\}$. Our choices for θ_s^* and ι_o^* are motivated by the results of [46, 47], which showed that this is the best-case orientation for determining the mass and radius of the source, with a 5% accuracy when the distance to the star is also known (as assumed here). The value of $\Delta\theta^*$ is chosen to enforce the point-like hot spot approximation, while we chose typical illustrative values for D^* and $k_B T^*$. Next, for EoS* we consider both a soft (SLy4) and a stiff (APR) EoS in order to test the variability of our constraints with the EoS. With an EoS* chosen, we choose ε_{15}^* to yield a neutron star with $1.93 M_\odot$ as, e.g. is the case of the neutron star in the PSR J1614–2230 binary [54, 55]. This choice is motivated by the observation that high-mass stars are more susceptible to the presence of the scalar field than low-mass ones (cf. Fig. 1). We also consider two values of f^* , 200 and 600 Hz, the latter to magnify the contributions of Doppler

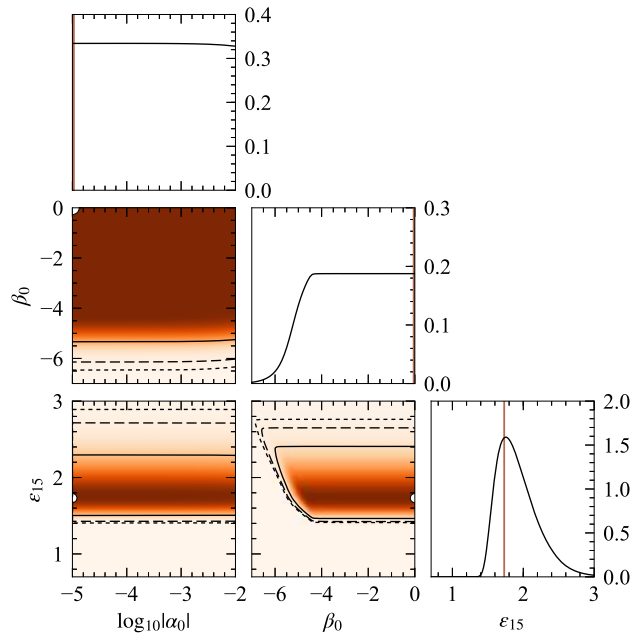


FIG. 2. Illustrative corner plot for the marginalized posterior distributions on the $\{\log_{10} |\alpha_0|, \beta_0, \varepsilon_{15}\}$ parameter space using EoS SLy4 and assuming a rotation frequency $f = 600$ Hz. In the color maps, the contours represent the 50% (solid line), 90% (dashed line) and 95% (dotted line) credible regions. The (white) circles indicate the injection values $\{-5, 0, 1.731\}$. These are indicated by the vertical lines in the panels showing the marginal posteriors. The results are qualitatively the same with EoS APR, albeit the constraints on $|\alpha_0|$ and β_0 are weakened when f is reduced and strengthened when we use this EoS (cf. Fig. 3).

and relativistic aberration effects on the pulse profile² [44, 58]. Finally, to generate our general relativistic injection, we set $\log_{10} |\alpha_0^*| = -5$ and $\beta_0^* = 0$ ³.

With these simplifications, our parameter space becomes three-dimensional, spanning only the central energy density ε_{15} and the theory parameters $\log_{10} |\alpha_0|$ and β_0 . For ε_{15} , we assume uniform priors in the ranges $\varepsilon_{15} \in [0.7, 3.0]$ (if EoS* = SLy4) and $\varepsilon_{15} \in [0.5, 2.4]$ (if EoS* = APR), which cover neutron star models with (roughly) minimum masses of $1 M_\odot$ and beyond the maximum mass for the corresponding EoS. For β_0 , we also use an uniform prior $\beta_0 \in [-7, 0]$, which includes the regime where spontaneous scalarization happens. The lower-bound already violates the best bounds from binary-pulsar observations by more than 1σ [24–26], whereas the upper bound is chosen to include the limit of general relativity. Finally, for $\log_{10} |\alpha_0|$ we choose an uniform prior $\log_{10} |\alpha_0| \in [-5, -2]$.

² For these large rotation frequencies one should include the influence of stellar oblateness in the model [56, 57] using e.g. the Oblate+Schwarzschild approximation [50, 51]. As shown in these papers, when θ_s, ι_o are close to the equator, the effects of oblateness on the pulse profile are suppressed, and we expect the same to be true in scalar-tensor gravity [14].

³ As noted earlier, these stars have $Q \approx 10^{-5}$ and are thus indistinguishable from neutron stars in general relativity as far as NICER is concerned.

The lower bound causes negligible changes to the structure of neutron stars, whereas the upper bound already violates the Cassini constraint by approximately one order of magnitude.

Having reduced our parameter space and chosen our priors, we calculate the best-fit parameters by minimizing the relative chi-squared between the injection and the model pulse profiles, scanning the parameter space using 16 phase stamps over the course of one stellar revolution. The standard deviation of the distribution $\sigma_{\varepsilon_{15}}$ is modeled as in [59, 60] and chosen to capture the optimistic 5% accuracy at which NICER can infer m and R . From the chi-squared, we calculate the likelihood function and from it we obtain the marginalized posterior distributions $p(\varepsilon_{15}|\mathbf{d})$, $p(\log_{10}|\alpha_0||\mathbf{d})$ and $p(\beta_0|\mathbf{d})$.

Figure 2 summarizes our results for $f^* = 600$ Hz and $\text{EoS}^* = \text{SLy4}$. The posterior of $\log_{10}|\alpha_0|$ is essentially flat, so little information is gained relative to the uniform prior. The posterior of β_0 is more interesting, clearly exhibiting a sharp decay that starts near the scalarization threshold at $\beta_0 \approx -4.35$. When $\beta_0 \gtrsim -4.35$, neutron stars are nearly identical to those of general relativity resulting in a flat marginal posterior in this region. However, when $\beta_0 \lesssim -4.35$, the conditions for spontaneous scalarization are realized, and, as neutron stars deviate more and more from their general relativity cousins as $\beta_0 \rightarrow -7$, they result in poor models to recover the injection, yielding an almost zero marginalized posterior when $\beta_0 = -7$. The posterior for ε_{15} peaks within $\lesssim 1\%$ from the injected value ε_{15}^* , with a slow decay as $\varepsilon_{15} \rightarrow 3$. This is because stars with the SLy4 EoS have a small variation in their radii and masses past the maximum mass ($\approx 2 M_\odot$), which is close to the injected value ($1.93 M_\odot$).

The conclusions above are robust to changes in the injected rotation frequency and the EoS. When we set f^* to 200 Hz and the EoS^* to APR, the likelihood surface does not change considerably, although the constraints on β are more stringent than when injecting SLy4, as summarized in Fig. 3. The latter shows the 68% credible regions in the $(|\alpha_0|, \beta_0)$ -plane for both EoS injections, which ought to be compared with the (1σ) constraints from Cassini and from the absence of scalar dipole radiation from the PSR J1738-0333 [24, 61], PSR J0348-0432 [62, 63] binaries [26] and the hierarchical triple system PSR J0348-1715 [27]. The contours reveal that for stiff equations of state (such as APR) the constraints on scalar-tensor gravity (in the $|\alpha_0| \rightarrow 0$ portion of the parameter space) from NICER observations can, in principle, be as strong as those obtained by binary pulsar observations⁴.

Let us further compare and contrast the qualitative behavior of the constraint contours of Fig. 3. As mentioned previously, β_0 is unconstrained from Solar System experiments, and therefore, the Cassini contour is constant at a fixed $|\alpha_0|$.

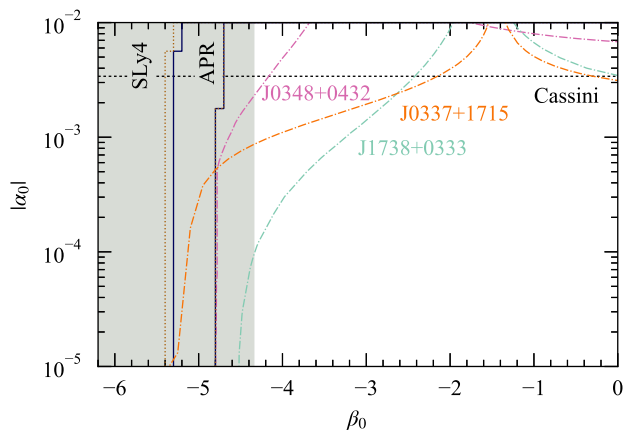


FIG. 3. Projected 1σ -constraints on (α_0, β_0) from pulse profile observations. In this plane, general relativity ($|\alpha_0| = 0, \beta_0 = 0$) is pushed infinitely down the ordinate. The shaded region covers the portion of the parameter space in which spontaneous scalarization happens. The solid (dashed) lines delimit the 68% credible regions for stars rotating with $f = 600$ (200) Hz, and different equations of state. For comparison, we also included the 68% credible regions from the Cassini mission [31] (dotted line) and the binary-pulsar systems J1738-0333, J0348-0432 [26] and the hierarchical triple system PSR J0337-1715 [27] (dot-dashed lines). The left-most part of our constraints lays on $\beta_0 = -4.8$ (for the APR EoS), indicating that pulse profile observations have the potential to marginally exclude strong-gravity phenomena as spontaneous scalarization, which in this particular theory requires $\beta_0 \lesssim -4.35$.

For binary pulsars, when $\beta_0 > -4.35$ neutron stars have small $Q \approx |\alpha_0|$, and the modification to the binary's orbital time decay \dot{P}_b scales with $|\alpha_0|^2$. But this modification is enhanced by two powers of the orbital velocity, which is of $\mathcal{O}(10^{-2} - 10^{-3})$, because the scalar field generates dipole radiation, instead of the quadrupole radiation of general relativity. The combination of these effects results in a modification to \dot{P}_b that can be constrained even for values of (α_0, β_0) beyond the threshold of scalarization and below the Cassini bound. Finally, in the NICER case, the modifications to the spacetime are controlled by Q , which is small and roughly independent of α_0 inside our prior range and outside the threshold of scalarization (i.e. outside the shaded region in Fig. 3). When scalarization does occur, however, Q acquires a non-perturbative enhancement, that leads to a large deviation from general relativity, and thus to nearly vertical constraint contours.

IV. CONCLUSIONS

NICER allows for the observation of x-ray pulse profiles from rotating neutron stars with unparalleled timing resolution. As the signal travels from the star to the detector, it probes the spacetime in the star's vicinity, opening the possibility of glimpsing (or constraining) deviations from general relativity in the strong-gravity regime. Using the tools developed in [14], we have explored whether such observations can place constraints on a concrete scalar-tensor gravity model

⁴ A note of caution is necessary when comparing the constraints obtained here and Refs. [26, 27] shown in Fig. 3. The constraints on β_0 depend critically on the choice of the prior range and a naïve comparison between the three works is strictly not correct. Moreover, the curves shown from [26] refer specifically to EoS SLy4, whereas the EoS used in [27] (labeled “0.2” in [64]) is considerably stiff, with a $2.6 M_\odot$ maximum mass in general relativity.

which admits large deviations from general relativity *only* in strong-gravity environments [29, 30].

As a proof-of-principle, we carried out a restricted likelihood analysis that suggests that (in principle) observations carried by NICER can constrain the parameter space of scalar-tensor gravity, severely restricting the domain in which spontaneous scalarization occurs. These projections are clearly preliminary but they do demonstrate, for the first time, the potential of including pulse profile observations as a new tool in the relativists' arsenal to perform strong-gravity tests. This is of interest not just for the ongoing NICER mission, but also for planned, future missions, such as the *Enhanced X-ray Timing and Polarimetry* mission [65]. Given these preliminary projections, *there is now strong justification to carry out a more detailed data analysis study that includes a more careful modeling of the instruments's response, as well as the covariances between all parameters in the model to determine how much degeneracies impact our ability to test general relativity.*

The encouraging results found here motivate the consideration of other questions. For instance, one could use both a general relativistic and a scalar-tensor model to analyze real NICER data. Using Bayesian analysis, one could then perform a model selection study to determine which theory is better supported by the data through the Bayes factor. Another important question is that of fundamental bias [66] in the parameter estimation of the properties of neutron stars. Pulse profile models assume *a priori* that general relativity is correct, which may bias parameter estimation, if the true underlying theory is not Einstein's. As a consequence, the mass and radius of the source could be systematically biased with immediate implications for EoS inference. This question could be investigated through a Bayesian analysis that uses a scalar-tensor theory pulse profile injection, but general relativity to model the data.

Still in the realm of synthetic data, a number of improvements can also be made. First, we could include beaming of the emitted radiation caused by Thomson scattering in the stellar atmosphere [46, 55–57]. Second, as radiation travels towards the observer, it interacts with the star's accretion disk [43] and the interstellar medium [55, 57]. Third, one could include background radiation [46, 55, 67] and generate synthetic data that is as realistic as possible. This data would then have to be convolved with the detector's response matrix, and combined with a Poisson sampling of the modeled pulse profile to determine the chi-squared through a Poisson likelihood [55]. With these ingredients taken into account, it would be interesting to verify whether the constraints on scalar-tensor gravity obtained here are *robust* to the assumptions we have made throughout the text. Regardless of the simplifications made here, our work nonetheless puts forward the enticing potential of probing strong-gravity with pulse profile observations.

Appendix A: Data analysis

In this appendix we present a brief overview of the methods used to obtain the projected constraints obtained in Sec. III.

We call the signal measured during an observation the *synthetic injected signal*, or (for brevity) *the injection* $F_{\text{inj}}(\theta^*)$. The pulse profile that we use to extract and characterize this observed pulse profile is referred to as *the model* $F_{\text{mod}}(\theta)$. Both pulse profiles can be calculated following [14] once all parameters $\theta = \{\varepsilon_{15}, \theta_s, \iota_0, \Delta\theta, D, k_B T, f, \text{EoS}, \log_{10} |\alpha_0|, \beta_0\}$ have been specified.

As discussed in the main text, we consider the reduced model parameter space obtained by fixing $\theta_{\text{fix}} = \{\theta_s, \iota_0, \Delta\theta, D, k_B T, f, \text{EoS}\}$ to the injected values, leaving as variable model parameters $\theta_{\text{var}} = \{\varepsilon_{15}, \log_{10} |\alpha_0|, \beta_0\}$

We calculate the best-fit parameter values by minimizing the reduced chi-squared χ_{red}^2 between the injection and the model pulse profiles, sampling over the model's variable parameters θ_{var} . The reduced chi-squared is defined as

$$\chi_{\text{red}}^2 \equiv \frac{1}{N} \sum_{i=1}^N \left[\frac{F_{\text{mod}}(\phi_i, \theta_{\text{fix}}, \theta_{\text{var}}) - F_{\text{inj}}(\phi_i, \theta_{\text{fix}}, \theta_{\text{var}}^*)}{\sigma(\phi_i)} \right]^2, \quad (\text{A1})$$

where the summation is over N time-stamps during the course of one revolution of the star. We normalize the phase over a revolution such that $\phi_i \in [0, 1]$, and use $N = 16$ time stamps. The standard deviation of the distribution σ is modeled as

$$\sigma(\phi_i) = \sigma_{\varepsilon_{15}}(\phi_i) + \sigma_{\log_{10} |\alpha_0|}(\phi_i) + \sigma_{\beta_0}(\phi_i), \quad (\text{A2})$$

where $\sigma_{\varepsilon_{15}}$, $\sigma_{\log_{10} |\alpha_0|}$ and σ_{β_0} are the standard deviations on each injected parameter $\theta_{\text{var}}^* = \{\varepsilon_{15}^*, \log_{10} |\alpha_0^*|, \beta_0^*\}$.

Since our injection is assumed to be consistent with general relativity, we set $\sigma_{\log_{10} |\alpha_0|} = \sigma_{\beta_0} = 0$, while the standard deviation $\sigma_{\varepsilon_{15}}$ is calculated by [59, 60]

$$\sigma_{\varepsilon_{15}}(\phi_i) = \frac{1}{2} \left| F_{\text{inj}}(\phi_i, \theta_{\text{fix}}, \{\varepsilon_{15}^* + \delta\varepsilon_{15}^+, \log_{10} |\alpha_0^*|, \beta_0^*\}) - F_{\text{inj}}(\phi_i, \theta_{\text{fix}}, \{\varepsilon_{15}^* - \delta\varepsilon_{15}^-, \log_{10} |\alpha_0^*|, \beta_0^*\}) \right|,$$

where (as explained in the main text) $\log_{10} |\alpha_0^*| = -5$ and $\beta_0^* = 0$, while $\delta\varepsilon_{15}^\pm$ remain to be specified. To obtain them, we start by assuming that $m^* = 1.93 M_\odot$ as discussed in the main text. Then, given an EoS, we calculate the central energy density ε_{15}^* for which this mass is obtained and record the corresponding radius R^* . Next, we draw a box in the mass-radius plane (in general relativity) centered at (m^*, R^*) with width spanning $R^*(1 \pm 0.05)$ and height spanning $m^*(1 \pm 0.05)$. The mass-radius curve intersects this box twice and these two points then determine $\delta\varepsilon_{15}^\pm$.

Once the reduced chi-squared is obtained, we calculate the likelihood

$$L(\theta_{\text{var}}) = \exp(-\chi_{\text{red}}^2/2). \quad (\text{A3})$$

When this is evaluated over the whole prior domain, we obtain the likelihood distribution shown in the off-diagonal panels of Fig. 2. Upon marginalization of the likelihood, we obtain the diagonal panels of the same figure.

To obtain the constraints shown in Fig. 3, we first sort our likelihood data in decreasing order of values of $L(\theta_{\text{var}})$. Then, we sum all the values of L (and record the corresponding θ_{var}) until 68% of the sum over *all* L -values is reached. The values of $\log_{10} |\alpha_0|$ and β_0 obtained from this procedure result in the dotted and solid lines in Fig. 3.

ACKNOWLEDGMENTS

We thank Anne Archibald, Justin Alsing, Alejandro Cárdenas-Avendaño, Neil Cornish, Cole Miller, Sharon Morsink, George Pappas and Hajime Sotani for valuable discussions. We also thank David Anderson for calculating and sharing with us the binary pulsar constraints. Finally,

we thank the anonymous referees for pertinent comments on our work. This work was supported by NASA grants NNX16AB98G and 80NSSC17M0041. Computational efforts were performed on the Hyalite High Performance Computing System, operated and supported by University Information Technology Research Cyberinfrastructure at Montana State University.

-
- [1] J. R. Oppenheimer and G. M. Volkoff, *Phys. Rev.* **55**, 374 (1939).
- [2] B. Abbott *et al.* (Virgo, LIGO Scientific), *Phys. Rev. Lett.* **119**, 161101 (2017), arXiv:1710.05832 [gr-qc].
- [3] M. Soares-Santos *et al.* (Dark Energy Camera GW-EM, DES), *Astrophys. J.* **848**, L16 (2017), arXiv:1710.05459 [astro-ph.HE].
- [4] B. P. Abbott *et al.* (Virgo, LIGO Scientific), *Phys. Rev. Lett.* **121**, 161101 (2018), arXiv:1805.11581 [gr-qc].
- [5] Z. Arzoumanian, S. Bogdanov, J. Cordes, K. Gendreau, D. Lai, J. Lattimer, B. Link, A. Lommen, C. Miller, P. Ray, R. Rutledge, T. Strohmayer, C. Wilson-Hodge, and K. Wood, in *astro2010: The Astronomy and Astrophysics Decadal Survey*, Vol. 2010 (2009) arXiv:0902.3264 [astro-ph.HE].
- [6] J. Poutanen, *AIP Conf. Proc.* **1068**, 77 (2008), arXiv:0809.2400 [astro-ph].
- [7] S. Bogdanov, J. E. Grindlay, and G. B. Rybicki, *Astrophys. J.* **689**, 407 (2008), arXiv:0801.4030 [astro-ph].
- [8] F. Özel, *Rept. Prog. Phys.* **76**, 016901 (2013), arXiv:1210.0916 [astro-ph.HE].
- [9] A. L. Watts *et al.*, *Rev. Mod. Phys.* **88**, 021001 (2016), arXiv:1602.01081 [astro-ph.HE].
- [10] N. Degenaar and V. F. Suleimanov, (2018), arXiv:1806.02833 [astro-ph.HE].
- [11] K. C. Gendreau, Z. Arzoumanian, and T. Okajima, in *Space Telescopes and Instrumentation 2012: Ultraviolet to Gamma Ray*, Proc. SPIE, Vol. 8443 (2012) p. 844313.
- [12] Z. Arzoumanian *et al.*, in *Space Telescopes and Instrumentation 2014: Ultraviolet to Gamma Ray*, Proc. SPIE, Vol. 9144 (2014) p. 914420.
- [13] K. Gendreau and Z. Arzoumanian, *Nature Astronomy* **1**, 895 (2017).
- [14] H. O. Silva and N. Yunes, *Phys. Rev.* **D99**, 044034 (2019), arXiv:1808.04391 [gr-qc].
- [15] T. Damour and G. Esposito-Farèse, *Class. Quant. Grav.* **9**, 2093 (1992).
- [16] T. Chiba, T. Harada, and K.-i. Nakao, *Prog. Theor. Phys. Suppl.* **128**, 335 (1997).
- [17] T. P. Sotiriou, *Lect. Notes Phys.* **892**, 3 (2015), arXiv:1404.2955 [gr-qc].
- [18] C. M. Will, *Living Rev. Rel.* **17**, 4 (2014), arXiv:1403.7377 [gr-qc].
- [19] E. Berti *et al.*, *Class. Quant. Grav.* **32**, 243001 (2015), arXiv:1501.07274 [gr-qc].
- [20] M. Kramer, *Int. J. Mod. Phys.* **D25**, 1630029 (2016), arXiv:1606.03843 [astro-ph.HE].
- [21] D. D. Doneva and G. Pappas, *Astrophys. Space Sci. Libr.* **457**, 737 (2018), arXiv:1709.08046 [gr-qc].
- [22] M. C. Miller and F. K. Lamb, *Astrophys. J.* **499**, L37 (1998), arXiv:astro-ph/9711325 [astro-ph].
- [23] H. Sotani, *Phys. Rev.* **D96**, 104010 (2017), arXiv:1710.10596 [astro-ph.HE].
- [24] P. C. C. Freire, N. Wex, G. Esposito-Farèse, J. P. W. Verbiest, M. Bailes, B. A. Jacoby, M. Kramer, I. H. Stairs, J. Antoniadis, and G. H. Janssen, *Mon. Not. Roy. Astron. Soc.* **423**, 3328 (2012), arXiv:1205.1450 [astro-ph.GA].
- [25] L. Shao, N. Sennett, A. Buonanno, M. Kramer, and N. Wex, *Phys. Rev.* **X7**, 041025 (2017), arXiv:1704.07561 [gr-qc].
- [26] D. Anderson, P. Freire, and N. Yunes, (2019), arXiv:1901.00938 [gr-qc].
- [27] A. M. Archibald, N. V. Gusinskaia, J. W. T. Hessels, A. T. Deller, D. L. Kaplan, D. R. Lorimer, R. S. Lynch, S. M. Ransom, and I. H. Stairs, *Nature* **559**, 73 (2018), arXiv:1807.02059 [astro-ph.HE].
- [28] K. Just, *Zeitschrift Naturforschung Teil A* **14**, 751 (1959).
- [29] T. Damour and G. Esposito-Farèse, *Phys. Rev. Lett.* **70**, 2220 (1993).
- [30] T. Damour and G. Esposito-Farèse, *Phys. Rev.* **D54**, 1474 (1996), arXiv:gr-qc/9602056 [gr-qc].
- [31] B. Bertotti, L. Iess, and P. Tortora, *Nature* **425**, 374 (2003).
- [32] D. Anderson and N. Yunes, (2019), arXiv:1901.00937 [gr-qc].
- [33] T. Harada, *Prog. Theor. Phys.* **98**, 359 (1997), arXiv:gr-qc/9706014 [gr-qc].
- [34] J. Novak, *Phys. Rev.* **D58**, 064019 (1998), arXiv:gr-qc/9806022 [gr-qc].
- [35] H. O. Silva, C. F. B. Macedo, E. Berti, and L. C. B. Crispino, *Class. Quant. Grav.* **32**, 145008 (2015), arXiv:1411.6286 [gr-qc].
- [36] T. Damour and K. Nordtvedt, *Phys. Rev. Lett.* **70**, 2217 (1993).
- [37] R. F. P. Mendes, *Phys. Rev.* **D91**, 064024 (2015), arXiv:1412.6789 [gr-qc].
- [38] H. O. Silva, J. Sakstein, L. Gualtieri, T. P. Sotiriou, and E. Berti, *Phys. Rev. Lett.* **120**, 131104 (2018), arXiv:1711.02080 [gr-qc].
- [39] D. D. Doneva and S. S. Yazadjiev, *Phys. Rev. Lett.* **120**, 131103 (2018), arXiv:1711.01187 [gr-qc].
- [40] L. Annulli, V. Cardoso, and L. Gualtieri, (2019), arXiv:1901.02461 [gr-qc].
- [41] F. Douchin and P. Haensel, *Astron. Astrophys.* **380**, 151 (2001), arXiv:astro-ph/0111092 [astro-ph].
- [42] A. Akmal, V. R. Pandharipande, and D. G. Ravenhall, *Phys. Rev.* **C58**, 1804 (1998), arXiv:nucl-th/9804027 [nucl-th].
- [43] J. Poutanen and M. Gierliński, *Mon. Not. Roy. Astron. Soc.* **343**, 1301 (2003), arXiv:astro-ph/0303084 [astro-ph].
- [44] J. Poutanen and A. M. Beloborodov, *Mon. Not. Roy. Astron. Soc.* **373**, 836 (2006), arXiv:astro-ph/0608663 [astro-ph].
- [45] H. Sotani, *Phys. Rev.* **D86**, 124036 (2012), arXiv:1211.6986 [astro-ph.HE].
- [46] K. H. Lo, M. C. Miller, S. Bhattacharyya, and F. K. Lamb, *Astrophys. J.* **776**, 19 (2013), arXiv:1304.2330 [astro-ph.HE].
- [47] K. H. Lo, M. C. Miller, S. Bhattacharyya, and F. K. Lamb, (2018), 10.3847/1538-4357/aaa95b, arXiv:1801.08031 [astro-ph.HE].
- [48] T. M. Braje, R. W. Romani, and K. P. Rauch, *Astrophys. J.* **531**, 447 (2000), arXiv:astro-ph/0004411 [astro-ph].

- [49] C. Cadeau, D. A. Leahy, and S. M. Morsink, *Astrophys. J.* **618**, 451 (2005), [arXiv:astro-ph/0409261 \[astro-ph\]](#).
- [50] C. Cadeau, S. M. Morsink, D. Leahy, and S. S. Campbell, *Astrophys. J.* **654**, 458 (2007), [arXiv:astro-ph/0609325 \[astro-ph\]](#).
- [51] S. M. Morsink, D. A. Leahy, C. Cadeau, and J. Braga, *Astrophys. J.* **663**, 1244 (2007), [arXiv:astro-ph/0703123 \[astro-ph\]](#).
- [52] D. Psaltis and F. Özel, *Astrophys. J.* **792**, 87 (2014), [arXiv:1305.6615 \[astro-ph.HE\]](#).
- [53] M. Baubock, D. Psaltis, and F. Özel, *Astrophys. J.* **811**, 144 (2015), [arXiv:1505.00780 \[astro-ph.HE\]](#).
- [54] E. Fonseca *et al.*, *Astrophys. J.* **832**, 167 (2016), [arXiv:1603.00545 \[astro-ph.HE\]](#).
- [55] M. C. Miller, *Astrophys. J.* **822**, 27 (2016), [arXiv:1602.00312 \[astro-ph.HE\]](#).
- [56] M. C. Miller and F. K. Lamb, *Astrophys. J.* **808**, 31 (2015), [arXiv:1407.2579 \[astro-ph.HE\]](#).
- [57] T. Salmi, N. J., and J. Poutanen, *Astron. Astrophys.* **618**, A161 (2018), [arXiv:1805.01149 \[astro-ph.HE\]](#).
- [58] H. Sotani and U. Miyamoto, *Phys. Rev.* **D98**, 103019 (2018), [arXiv:1811.03702 \[astro-ph.HE\]](#).
- [59] D. Ayzenberg, K. Yagi, and N. Yunes, *Class. Quant. Grav.* **33**, 105006 (2016), [arXiv:1601.06088 \[astro-ph.HE\]](#).
- [60] D. Ayzenberg and N. Yunes, *Class. Quant. Grav.* **34**, 115003 (2017), [arXiv:1701.07003 \[gr-qc\]](#).
- [61] J. Antoniadis, M. H. van Kerkwijk, D. Koester, P. C. C. Freire, N. Wex, T. M. Tauris, M. Kramer, and C. G. Bassa, *Mon. Not. Roy. Astron. Soc.* **423**, 3316 (2012), [arXiv:1204.3948 \[astro-ph.HE\]](#).
- [62] M. Kramer *et al.*, *Science* **314**, 97 (2006), [arXiv:astro-ph/0609417 \[astro-ph\]](#).
- [63] M. Kramer and N. Wex, *Classical and Quantum Gravity* **26**, 073001 (2009).
- [64] P. Haensel, M. Proszynski, and M. Kutschera, *A&A* **102**, 299 (1981).
- [65] J. J. M. in 't Zand *et al.* (eXTP), *Sci. China Phys. Mech. Astron.* **62**, 029506 (2019), [arXiv:1812.04023 \[astro-ph.HE\]](#).
- [66] N. Yunes and F. Pretorius, *Phys. Rev.* **D80**, 122003 (2009), [arXiv:0909.3328 \[gr-qc\]](#).
- [67] F. Özel, D. Psaltis, Z. Arzoumanian, S. Morsink, and M. Baubock, *Astrophys. J.* **832**, 92 (2016), [arXiv:1512.03067 \[astro-ph.HE\]](#).